Modern numerical differentiation technique for extracting nucleon momentum distributions

Tongqi Liang ,[1] Dong Bai ,[2] and Zhongzhou Ren[1,3,*]

[1] *School of Physics Science and Engineering, Tongji University, Shanghai 200092, China*

[2] *College of Mechanics and Engineering Science, Hohai University, Nanjing 211100, Jiangsu, China*

[3] *Key Laboratory of Advanced Micro-Structure Materials, Ministry of Education, Shanghai 200092, China*

(Received 23 January 2024; revised 13 March 2024; accepted 9 April 2024; published 13 May 2024)

Numerical differentiation is crucial for extracting reliable nucleon momentum distributions (NMDs) from cross section data of inclusive electron scattering within the framework of y scaling. A naive application of the traditional finite difference approach to noisy experimental data may lead to negative values and suspect fluctuations in NMDs at high momenta. To solve this problem, we propose using a sophisticated modern technique known as smoothing spline for numerical differentiation, which has a number of advantages over the traditional approach and gives NMDs more compatible with physical considerations. We extract new NMDs for the deuteron and study their scaling behaviors with respect to the nucleon momentum k. It is found that NMDs may follow piecewise scaling laws with $n(k) \sim 1/k^5$ for $0.25 < k < 0.6$ GeV/c and $n(k) \sim 1/k^7$ for $0.6 < k < 1.2$ GeV/c.

DOI: 10.1103/PhysRevC.109.054313

I. INTRODUCTION

Nucleon momentum distributions (NMDs) quantify the probability of nucleons taking specific momenta in nuclear systems. They play a fundamental role in nuclear physics and offer crucial insights into the nature of nuclear forces [1–5]. Experimentally, they can be extracted from cross section data of inclusive quasielastic electron-nucleus scattering [6–11]. A leading framework for this task is y scaling based on the plane wave impulse approximation (PWIA) [12–18], which relates the NMD $n(k)$ to the first-order derivative of a special single-variable function known as the scaling function $F(y)$,

$$n(k) = -\frac{1}{2\pi y}\frac{dF(y)}{dy}\bigg|_{|y|=k}. \qquad (1)$$

Here, k is the nucleon momentum, and y is the so-called scaling variable which can be interpreted as the minimal momentum of nucleons knocked out of the nucleus by the electron [19]. As shown later in Sec. II A, $F(y)$ and y can be derived directly from experimental observables including inclusive cross sections, electron momentum transfer, and electron energy transfer, based on which the experimental extraction of $n(k)$ is finally achieved. In the literature, the experimental NMDs have been extracted for the deuteron, ^{3,4}He, ^{12}C, and ^{56}Fe in this way [8,20]. They act as benchmarks to compare and evaluate different proposals of realistic nuclear forces [21,22].

In this work, we focus on an important yet easily overlooked aspect of the experimental extraction of NMDs based on y scaling, the implementation of the first-order derivative $dF(y)/dy$ in Eq. (1). As mentioned before, the scaling function $F(y)$, from which the NMD is extracted, can be derived from cross section data. The experimental $F(y)$ takes values at discrete points of y (see Fig. 2), and the first-order derivative $dF(y)/dy$ has to be calculated in a numerical way. Maybe, the simplest way to do this is to employ finite difference [8],

$$\frac{dF(y)}{dy}\bigg|_{y=y_i} \approx \frac{F(y_{i+1}) - F(y_i)}{y_{i+1} - y_i}, \qquad (2)$$

where $\{(y_i, F(y_i))\}$ is the ith data point derived from experimental data. Moreover, this would be a satisfactory choice if the data points are of large numbers and of high quality. However, the real situation can be different. For example, at high momenta above the Fermi momentum k_F, the number and quality of data points are both reduced compared to those at low momenta below k_F [7]. It turns out that these issues may lead to negative values and suspect fluctuations in NMDs at high momenta [see Fig. 3(b)]. Can this situation be improved by adopting more sophisticated numerical differentiation techniques?

We propose that a modern numerical differentiation technique known as smoothing spline could provide a positive answer to the above question [23,24]. It has a number of advantages in dealing with noisy data points compared to a naive application of finite difference and many other numerical differentiation techniques (e.g., Gaussian smoothing [25] and Savitzky-Golay smoothing [26,27]). First, it has few hyperparameters that cannot be determined by the data set and the underlying physics [28,29]. Second, it does not assume any specific functional form to describe complex correlations between data points, making it flexible and adaptive in modeling data. Third, it is effective at handling noisy data, providing a reliable extraction of the underlying trends and

*zren@tongji.edu.cn

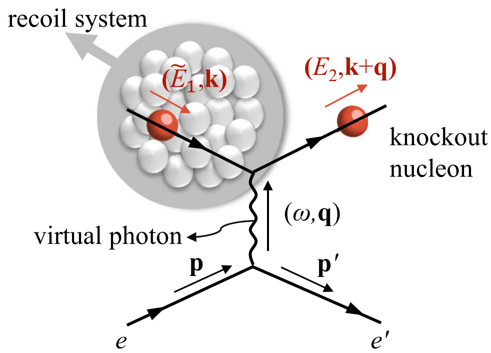

FIG. 1. A typical one-nucleon knockout process in quasielastic electron-nucleus scattering under the assumption of PWIA.

patterns. Smoothing spline has been widely used in biology [30], chemistry [24,29], ecology [31], epidemiology [32], and many other disciplines. However, it is fair to say that smoothing spline is less known in nuclear physics. Especially, as far as we know, it has not been applied to the experimental extraction of NMDs.

The rest parts of the article are organized as follows: In Sec. II, the frameworks of y scaling and smoothing spline are introduced. In Sec. III, smoothing spline is applied to the NMD extraction for the deuteron, with the nucleon momentum k up to 1.2 GeV/c. A detailed comparison is made to both the finite difference extraction of NMD and *ab initio* calculations in order to justify the reliability and advantage of smoothing spline. Special attention is also paid to the scaling behaviors of the NMD with respect to k. In Sec. IV, conclusions are drawn.

II. THEORETICAL FRAMEWORK

A. y scaling

In PWIA, it is assumed that only one nucleon is knocked out at one time in quasielastic electron-nucleus scattering, without interacting with the recoil system [13]. Such a one-nucleon knockout process is illustrated in Fig. 1, along with the meanings of relevant kinematic variables. The inclusive cross section $\frac{d^2\sigma}{d\omega d\Omega}$ is then given by the product of the single-nucleon cross section $\sigma_{ep(en)}$ and the so-called nuclear structure function $F(q,\omega)$,

$$\frac{d^2\sigma}{d\omega\, d\Omega} = (Z\sigma_{ep} + N\sigma_{en})\left|\frac{\partial\omega}{k\,\partial\cos\alpha}\right|^{-1} F(q,\omega). \quad (3)$$

Here, $k = |\mathbf{k}|$ is the nucleon momentum, $q = |\mathbf{q}|$ and ω are the momentum transfer and the energy transfer of the electron, Z and N are the numbers of protons and neutrons in the target nucleus, and $|\frac{\partial\omega}{k\,\partial\cos\alpha}|^{-1}$ (with $\cos\alpha = \frac{\mathbf{q}\cdot\mathbf{k}}{qk}$) is the kinematic factor resulting from the energy conservation in the scattering process. The single-nucleon cross sections σ_{ep} and σ_{en} can be found in Ref. [33],

$$\sigma_{ep(en)} = \frac{\sigma_M}{E_1E_2}\left\{\left(\frac{Q^2}{q^2}\right)^2\left[\frac{(E_1+E_2)^2}{4}\left(F_1^2+\bar{\tau}F_2^2\right) - \frac{q^2}{4}(F_1+F_2)^2\right]\right.$$
$$\left. + \left(\tan^2\frac{\theta}{2} + \frac{Q^2}{2q^2}\right)\left[p'^2\sin^2\alpha\left(F_1^2+\bar{\tau}F_2^2\right) + \frac{\bar{Q}^2}{2}(F_1+F_2)^2\right]\right\}, \quad (4)$$

where E_1 and E_2 are given by $E_1 = \sqrt{m_N^2+k^2}$ and $E_2 = \sqrt{m_N^2+(\mathbf{k}+\mathbf{q})^2}$, with m_N being the nucleon mass, θ is the electron scattering angle, p' is the momentum of the knockout nucleon, $Q^2 = q^2-\omega^2$, $\bar{Q}^2 = q^2-(E_1-E_2)^2$, and $\bar{\tau} = \bar{Q}^2/(4m_N^2)$ are three auxiliary kinematic variables, and σ_M is the Mott cross section. The elastic proton and neutron form factors F_1 and F_2 are taken from Refs. [34,35]. The nuclear structure function $F(q,\omega)$ is expressed as the integral of the nucleon spectral function $P_N(k,E)$,

$$F(q,\omega) = 2\pi\int_{E_{\min}}^{E_{\max}(q,\omega)} dE \int_{k_{\min}(q,\omega,E)}^{k_{\max}(q,\omega,E)} k\,P_N(k,E)\,dk\ , \quad (5)$$

where $E_{\min(\max)}$ and $k_{\min(\max)}$ are respectively the minimal (maximal) energy and momentum of nucleons when they are knocked out from the nucleus by the electron. The nucleon spectral function $P_N(k,E)$ represents the joint probability distribution to find a nucleon with momentum k and removal energy E in the nucleus.

Provided that the recoil system is not excited, i.e., $E = E_{\min}$, $k_{\min}$ depends only on q and ω, and is renamed as the scaling variable y

$$|y| = k_{\min}(q,\omega,E_{\min}). \quad (6)$$

The scaling variable y can be determined from the energy conservation

$$\omega + M_A = \left[m_N^2+(q+y)^2\right]^{1/2} + \left(M_{A-1}^2+y^2\right)^{1/2}, \quad (7)$$

where M_A and M_{A-1} denote the masses of the target nucleus and the recoil system. In terms of the scaling variable y, the kinematic factor $|\frac{\partial\omega}{k\,\partial\cos\alpha}|^{-1}$ in Eq. (3) is given by

$$\left|\frac{\partial\omega}{k\,\partial\cos\alpha}\right|^{-1} = \frac{\sqrt{m_N^2+(q+y)^2}}{q}. \quad (8)$$

As $P_N(k,E)$ decreases rapidly with the increase of k and E, $E_{\max}$ and $k_{\max}$ in Eq. (5) can be safely substituted by infinity. In the large Q^2 limit, the structure function becomes the scaling function $F(y)$ which only depends on the scaling variable y,

$$F(y) = 2\pi\int_{E_{\min}}^{\infty} dE \int_{|y|}^{\infty} k\,P_N(k,E)\,dk. \quad (9)$$

For the deuteron, the recoil system has no excitation energy and the removal energy E is the minimal separation energy $E_{\min} = 2.225$ MeV. The spectral function is then given by the approximate form $P_N(k, E) = n(k)\delta(E - E_{\min})$ and thus entirely determined by the nucleon momentum distribution $n(k)$. The scaling function $F(y)$ becomes

$$F(y) = 2\pi \int_{|y|}^{\infty} n(k)\, k\, dk, \tag{10}$$

where the nucleon momentum distribution is

$$n(k) = \int_{E_{\min}}^{\infty} P_N(k, E)\, dE. \tag{11}$$

Eventually, the master formula for the y-scaling approach to the NMD extraction is obtained from Eq. (10),

$$n(k) = -\frac{1}{2\pi y} \frac{dF(y)}{dy}\bigg|_{|y|=k}, \tag{12}$$

where the scaling function $F(y)$ can be extracted from the inclusive cross sections with the help of Eq. (3).

B. Smoothing spline

Consider an experimental data set with $N + 1$ discrete points$\{(x_i, y_i)\}$ $(i = 0, \ldots, N)$. In principle, y_i consists of the true value $f(x_i)$ and the noise part $\eta(x_i)$, i.e.,

$$y_i = f(x_i) + \eta(x_i). \tag{13}$$

The main goal of numerical difference methods is to obtain a good estimation of derivatives of $f(x_i)$ from $\{(x_i, y_i)\}$. In the smoothing spline method, this is done as follows. Let $\tilde{f}(x)$ be an estimation of $f(x)$ within the interval of $a < x < b$. In smoothing spline, $\tilde{f}(x)$ is constructed by minimizing the penalized least-squares loss function [23]

$$\sum_{i=0}^{N} \{y_i - \tilde{f}(x_i)\}^2 + \lambda^{-1} \int_a^b \{\tilde{f}''(x)\}^2 dx, \tag{14}$$

in the functional space of all functions with square-integrable second derivatives. The first term calculates the least-squares error, while the second term is referred to as the penalty functional to assess the function's smoothness. The smoothness parameter λ manages the tradeoff between the function's smoothness and the least-squares fit.

From the corresponding Euler-Lagrange equations, the optimal function $\tilde{f}(x)$ satisfies the following conditions [23]:

$$\tilde{f}^{(4)}(x) = 0, \quad x_i < x < x_{i+1}, \quad i = 0, \ldots, N - 1, \tag{15}$$

$$\tilde{f}^{(k)}(x_i)_- - \tilde{f}^{(k)}(x_i)_+ = \begin{cases} 0 & \text{if} \quad k = 0, 1, 2, \\ 2\lambda[\tilde{f}(x_i) - y_i] & \text{if} \quad k = 3, \end{cases} \tag{16}$$

with $\tilde{f}^{(k)}(x_i)_\pm = \lim_{h\to 0} \tilde{f}^{(k)}(x_i \pm h)$ being the left (right) kth order derivative of $\tilde{f}(x)$ at the point x_i. The boundary conditions at x_0 and x_N can be found in Ref. [23].

Equations (15) and (16) demonstrate that $\tilde{f}(x)$ is composed of cubic parabolas,

$$\tilde{f}(x) = a_i + b_i(x - x_i) + c_i(x - x_i)^2 + d_i(x - x_i)^3, \tag{17}$$

within the range $x_i \leqslant x < x_{i+1}$. The above equation joins at common endpoints such that $\tilde{f}(x)$, $\tilde{f}'(x)$, and $\tilde{f}''(x)$ are continuous. Consequently, the solution $\tilde{f}(x)$ in Eq. (14) is a cubic spline. The procedure of minimizing the penalized least-squares loss function in Eq. (14) converts to solve the spline coefficients $\{(a_i, b_i, c_i, d_i)\}$.

Inserting Eq. (17) into (16), the relations of the spline coefficients can be obtained. Utilizing the condition of $\tilde{f}'(x_i)_\pm$, one can obtain

$$T\mathbf{c} = Q^T\mathbf{a}. \tag{18}$$

The superscript "T" represents transpose. Applying the condition of $\tilde{f}'''(x_i)_\pm$, one can derive the relation

$$Q\mathbf{c} = \lambda(\mathbf{y} - \mathbf{a}). \tag{19}$$

Q is a tridiagonal matrix with $N + 1$ rows and $N - 1$ columns. T is a positive definite tridiagonal matrix of order $N - 1$. The nonzero matrix elements of Q and T are defined as

$$\begin{aligned} &Q_{i-1,i} = 1/h_{i-1}, \quad Q_{i,i} = -1/h_{i-1} - 1/h_i, \\ &Q_{i+1,i} = 1/h_i, \quad T_{i,i} = 2(h_{i-1} + h_i)/3, \\ &T_{i,i+1} = T_{i+1,i} = h_i/3, \end{aligned} \tag{20}$$

with $h_i = x_{i+1} - x_i$ and $i = 1, \ldots, N - 1$. The vectors in Eqs. (18) and (19) are defined as

$$\begin{aligned} \mathbf{c} &= \{c_1, \ldots, c_{N-1}\}^T, \\ \mathbf{y} &= \{y_0, y_1, \ldots, y_N\}^T, \\ \mathbf{a} &= \{a_0, a_1, \ldots, a_N\}^T. \end{aligned} \tag{21}$$

By solving Eqs. (18) and (19), $\mathbf{c}$ and $\mathbf{a}$ are written as

$$\begin{aligned} (Q^T Q + \lambda T)\mathbf{c} &= \lambda Q^T \mathbf{y}, \\ \mathbf{a} &= \mathbf{y} - \lambda^{-1} Q\mathbf{c}. \end{aligned} \tag{22}$$

Then the explicit form of vector $\mathbf{a}$ is expressed as

$$\mathbf{a} = \mathbf{y} - Q(Q^T Q + \lambda T)^{-1} Q^T \mathbf{y}. \tag{23}$$

Noticing that $\tilde{f}(x) = a_i$ at $\{x_i\}$ from Eq. (17), only the vector $\mathbf{a}$ is needed for the estimations at $\{x_i\}$. The estimation of $\tilde{\mathbf{f}} = [\tilde{f}(x_0), \ \ldots, \ \tilde{f}(x_N)]^T$ can be addressed in matrix form,

$$\tilde{\mathbf{f}} = \mathbf{a} = A(\lambda)\,\mathbf{y}, \tag{24}$$

where $A(\lambda) = I - Q(Q^T Q + \lambda T)^{-1} Q^T$ is the so-called influence matrix and I is the $(N + 1) \times (N + 1)$ unit matrix. Thus, one can choose a smoothness parameter λ and obtain the estimations. A smaller value of λ means a more pronounced level of smoothness.

Researchers often resort to an *ad hoc* procedure when faced with the task of selecting parameters. One popular choice to determine λ is generalized cross-validation (GCV) [28], where the estimation of the nth point is determined by fitting a smooth trend line to all the data points except the nth one. GCV works by minimizing the sum of squared differences $V(\lambda)$ between the nth data point and its estimated value. For the case of cubic smoothing spline, $V(\lambda)$ is given by the influence matrix $A(\lambda)$,

$$V(\lambda) = \frac{||[I - A(\lambda)]\mathbf{y}||^2}{[N + 1 - \mathrm{Tr}A(\lambda)]^2}, \tag{25}$$

where $||\cdot||$ represents the $\mathcal{L}_2$-norm and $\mathrm{Tr}A(\lambda)$ calculates the trace of the influence matrix.

In this work, we adopt cubic smoothing spline for the numerical derivative and utilize GCV to optimize the smoothing parameter such that no parameter inputs are needed. It should be emphasized that the smoothing spline method differs from the concepts of interpolation and curve fitting. The interpolating method generates results passing through every data point, which is a horrible scenario for experimental data with noise. Curve fitting is a helpful method to handle noisy experimental data in extracting NMDs and can yield reasonable results [36,37]. However, the necessity to predefine functional form may bring some extent of model dependence. Moreover, curve fitting is less effective in capturing local features than smoothing spline, which can retain more information in the data.

III. NUMERICAL RESULTS

NMDs provide a key window in validating the fundamental nucleon-nucleon (NN) interactions. They can be extracted from the experimental inclusive cross sections by utilizing the y-scaling analysis. As shown in Sec. II A, experimental NMDs are obtained by taking the first-order derivative of the scaling function $F(y)$ concerning the scaling variable y, with $F(y)$ extracted from the experimental cross sections. However, the experimental data are invariably corrupted by noise, and a naive finite difference approach can amplify this noise, leading to negative values and suspect fluctuations in NMDs at high momenta [8,11]. This work tackles the numerical differentiation problem by applying a nonparametric technique, known as smoothing spline. We focus on the NMDs of the deuteron because the high-momentum tails of medium to heavy nuclei are proportional to those of the deuteron [38]. The experimental data utilized in this paper are measured at sufficiently high Q^2 values [6–8].

A. NMD extractions for the deuteron by applying smoothing spline

Shown in Fig. 2 are the results of the scaling function $F(y)$ of the deuteron by using smoothing spline. The 68.3% confidence interval is calculated using Bayesian estimation [39]. The experimental cross sections, from which the scaling function is derived, are measured at the electron energy $E = 4.045$ GeV and scattering angle $\theta = 37^\circ$ with $Q^2 = 3.5\ (\mathrm{GeV/c})^2$ at the quasielastic peak [6]. The $F(y)$ results derived from the cross section data without applying smoothing spline are also shown. It can be seen that the smoothing spline method effectively handles the noisy data for large negative y values. The curve passes through bunches of squares and ensures that they are uniformly distributed on both sides of the smoothed curve. The smoothing spline method can simultaneously minimize the least-squares deviation and estimate the smoothness of the curve within the whole interval. The

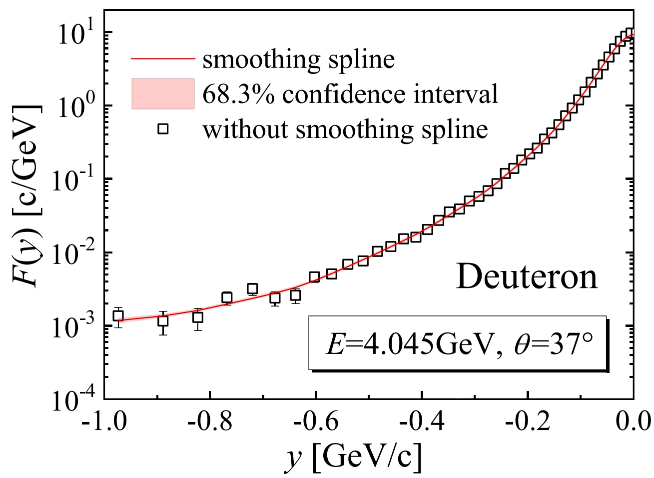

FIG. 2. Scaling function $F(y)$ of deuteron by applying smoothing spline (solid red line) extracted from the inclusive cross sections. The cross section data are measured at the electron energy $E = 4.045$ GeV and scattering angle $\theta = 37^\circ$ with $Q^2 = 3.5\ (\mathrm{GeV}/c)^2$ at the quasielastic peak [6]. The corresponding light red band represents the 68.3% confidence interval. Note that the confidence interval is so narrow that it is not visually apparent in the figure. The squares represent the $F(y)$ results derived from the cross section data without applying smoothing spline.

smoothness parameter λ is needed in the smoothing spline method to control the smoothness. To remove the uncertainty associated with selecting λ and provide robust smoothed results, the optimal λ is determined by utilizing GCV in this work. Then the smoothing spline method is carried out in a nonparametric manner. It is noted that the smoothing spline method minimizes the least-square errors as a whole. The experimental cross sections in low-ω regions, which correspond to the high-momentum nucleons and have small values, have little contribution. GCV fails to give an optimal λ for the experimental data in low-ω regions. To overcome this issue, a logarithmic scale is used to process the experimental data in this study when applying GCV to determine the optimal λ value in the smoothing spline method.

By taking the first derivative of $F(y)$ with respect to y in Fig. 2, the new NMD results for the deuteron given by smoothing spline are derived and displayed in Fig. 3(a). The $n(k)$ results by applying the finite difference method are also shown in the same figure. The uncertainties of $F(y)$ are propagated to $n(k)$. In this paper, a Gaussian profile is assumed for each point of $F(y)$, centered around the measured values with a width given by the uncertainty. The resulting $n(k)$ values also follow a Gaussian distribution and uncertainties of $n(k)$ can be estimated [11,40]. The same procedure is also applied to the 68.3% confidence interval of new NMDs given by smoothing spline. Theoretical results of $n(k)$ calculated by the quantum Monte Carlo (QMC) methods with three NN interactions, AV18, NV2-Ia, and NV2-IIb, are shown in the same figure for comparison [1]. The new NMDs obtained with smoothing spline are smoother when compared to the $n(k)$ results extracted using the finite difference method. These NMDs also eliminate suspect fluctuations caused by noise. Furthermore,

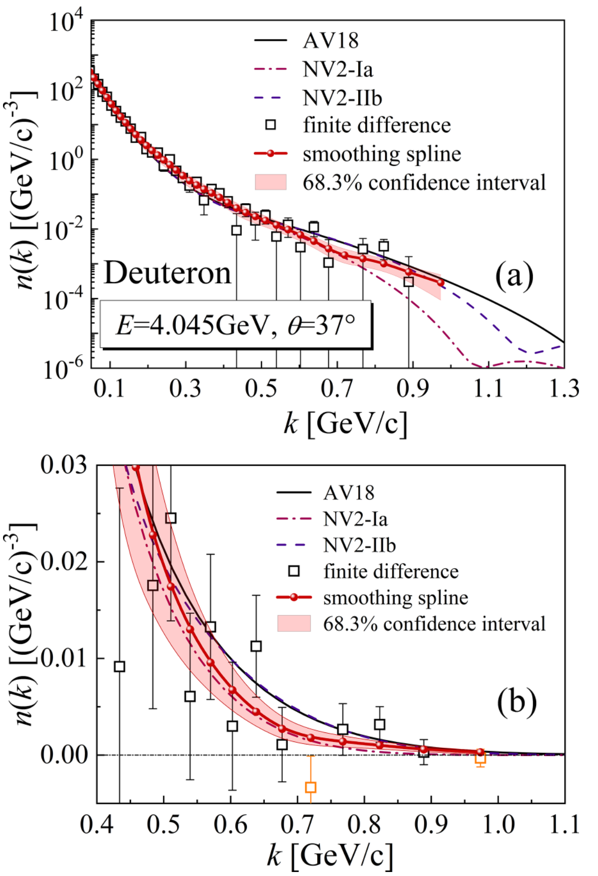

FIG. 3. (a) New NMDs $n(k)$ of the deuteron by applying smoothing spline (solid red line with balls), extracted from scaling functions in Fig. 2 based on y scaling. The light red band represents the 68.3% confidence interval. The squares show the NMD results by applying the finite difference method. The theoretical QMC calculations with different NN interactions (lines) are also presented [1]. (b) Similar to (a), but focusing on the momentum region of $0.4 < k < 1.1$ GeV/c. Two orange squares indicate the NMD data points with negative values, which are missing in (a) plotted on a logarithmic scale.

the new NMDs coincide with the QMC calculations and are positioned between the three QMC calculations employing different NN interactions at higher momenta.

In PWIA, the scaling function $F(y)$, as expressed in Eq. (10), signifies the integral of the nucleon momentum distribution from y to infinity. It is expected to exhibit a monotonic decrease as $|y|$ increases. However, as shown in Fig. 2, the experimental cross sections fail to produce monotonic $F(y)$ as noise always exists. Therefore negative values of $n(k)$ are generated as stated in Eq. (1). $n(k)$ points with negative values are more likely to occur in high-momentum regions. Figure 3(b) provides a detailed view of the $n(k)$ results in the region of $0.4 < k < 1.1$ GeV/c. It is shown in Fig. 3(b) that two negative $n(k)$ points are given by the finite difference method (specifically at $k = 0.72$ and 0.97 GeV/c), which are missing in Fig. 3(a) plotted on a logarithmic scale. The smoothing spline method recovers the monotonicity of $F(y)$ and avoids negative values of $n(k)$.

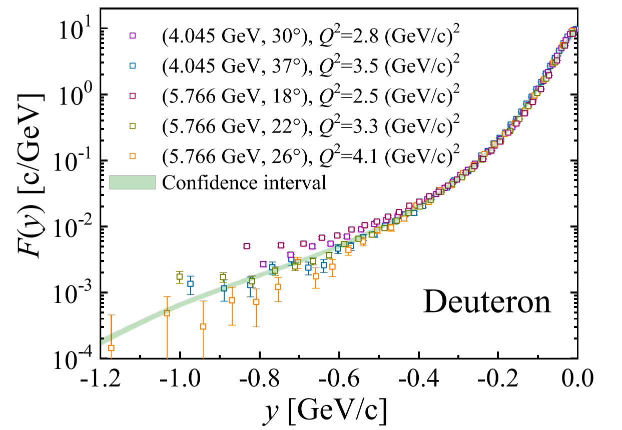

FIG. 4. Scaling function $F(y)$ of the deuteron (squares) extracted from the experimental data measured at $(E, \theta) =$ (4.045 GeV, 30°), (4.045 GeV, 37°), (5.766 GeV, 18°), (5.766 GeV, 22°), and (5.766 GeV, 26°) [6,8]. The Q^2 values at the quasielastic peak are also shown. The color band represents the uncertainties associated with the y-scaling violations estimated by the smoothing spline method.

In the impulse approximation, the scaling limit is assumed to be reached at large Q^2 values and the scaling function depends on only one variable, which is directly related to the NMD [8]. However, the impulse approximation picture breaks down when the effects of the rescattering of the knockout nucleon and nucleon-nucleon correlations are included [37,41–43]. Moreover, in Ref. [44] the authors found potentially large contributions of meson-exchange currents (MECs) on scaling functions at large negative y. These effects may lead to non-negligible y-scaling violations in the region of large negative y values and hamper the unambiguous extraction of NMDs at high momenta. In the following we assess the impact of y-scaling violations at large negative y using extensive experimental data and provide more convincing NMD results.

Shown in Fig. 4 are the scaling functions extracted from all the existing experimental data that can provide scaling results for $|y| > 0.8$ GeV/c [6,8]. The corresponding values of the incident energy E, scattering angle θ, and Q^2 at the quasielastic peak are shown in the figure. In the region $0 < |y| < 0.5$ GeV/c, scaling functions show highly consistent results, while apparent scaling violations occur at large negative y due to the mechanisms beyond the impulse approximation. The confidence interval, represented by the color band, is given by smoothing spline to quantify the amount of scaling violations. Notice that the confidence interval aims to contain the true function values with 95.5% probability.

Theoretical QMC calculations of $n(k)$ with different NN interactions exhibit significant variations in their high-momentum tails because the tensor force and the short-range repulsion are poorly described [1]. Imposing constraints on the high-momentum tail is a significant and difficult task in nuclear physics. Utilizing the $F(y)$ results in Fig. 4, new NMD results are extracted by applying smoothing spline and presented in Fig. 5 to mitigate the stochasticity of a single experimental dataset. The color band is propagated from $F(y)$ results and associated with the y-scaling violations. The error bar indicates the 68.3% confidence interval for each

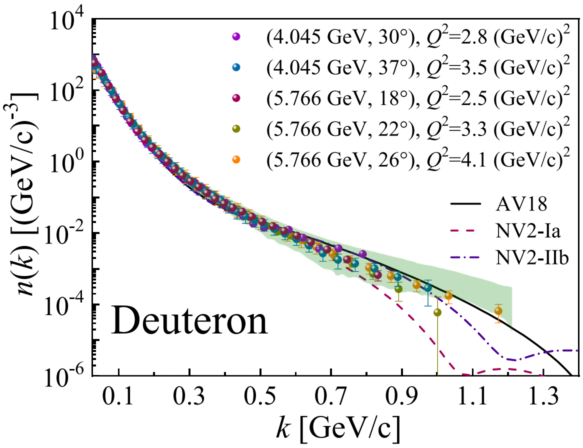

FIG. 5. New NMDs $n(k)$ of the deuteron given by smoothing spline (balls) extracted from the experimental cross sections measured at $(E, \theta) = (4.045$ GeV, $30^\circ)$, (4.045 GeV, 37°), (5.766 GeV, 18°), (5.766 GeV, 22°), and (5.766 GeV, 26°) [6,8]. The Q^2 values at the quasielastic peak are also shown. The error bar indicates the 68.3% confidence interval for each data set. The color band is associated with the y-scaling violations. The lines represent the theoretical QMC calculations with different NN interactions [1].

data set. The smoothing spline method avoids the negative values of $n(k)$ for these data sets. Furthermore, it extends the experimental $n(k)$ results up to $k \approx 1.2$ GeV/c. Three QMC calculations coincide with new experimental $n(k)$ for $k < 0.6$ GeV/c. However, in the higher-momentum region, distinctions occur for the QMC calculations using different NN interactions. The experimental $n(k)$ results are located between these calculations. It is challenging to discern which NN interaction yields superior results with the existing data.

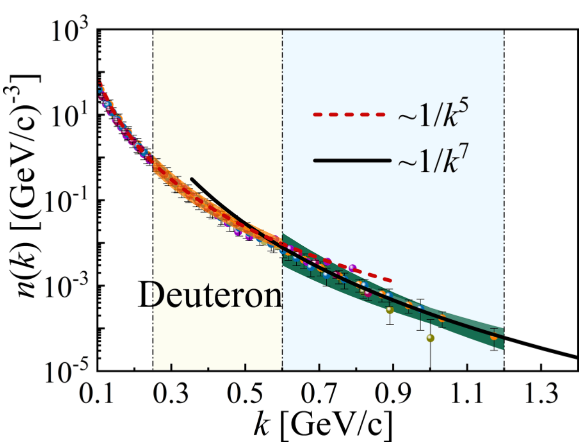

FIG. 6. Scaling behaviors of the high-momentum tail. The new $n(k)$ results (balls) are the same as those in Fig. 5. The dashed red line illustrates the fitting of $n(k)$ results in the region $0.25 < k < 0.6$ GeV/c, suggesting a scaling behavior of $n(k) \sim 1/k^5$. The solid black line represents the scaling behavior of $n(k) \sim 1/k^7$ by fitting the $n(k)$ results in the region $0.6 < k < 1.2$ GeV/c. The orange and green bands depict the loci of the 95% confidence bounds of the fitted curves.

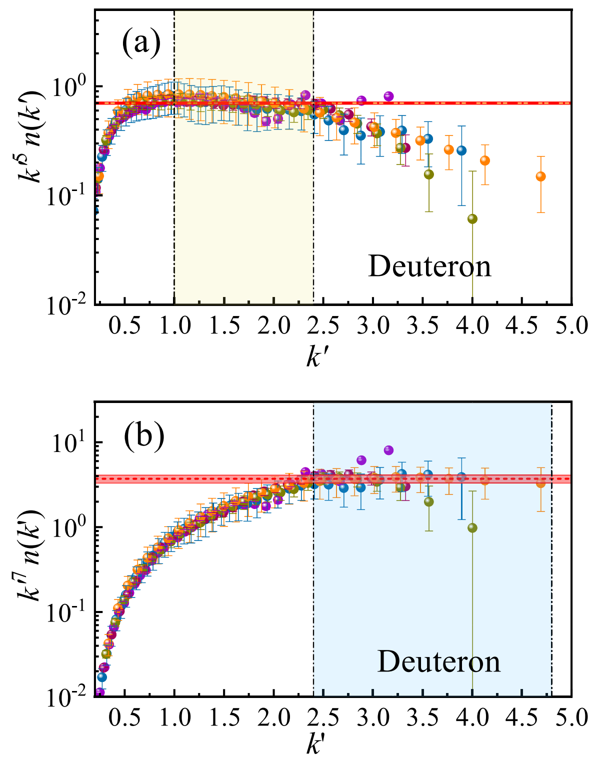

FIG. 7. Scaled NMDs (a) $k'^5\, n(k')$ and (b) $k'^7\, n(k')$ with $k' = k/k_F$. The new $n(k)$ results (balls) are the same as those in Fig. 5. The data points are plotted in units of $k_F = 250$ MeV/c, the typical Fermi momentum for medium and heavy nuclei. The dashed red lines demonstrate the plateaus by fitting the scaled NMD data, and the light red bands represent the 95% confidence bounds of the linear fitted curves.

B. Scaling behaviors

The behavior of high-momentum tails significantly influences the properties of nuclear matter, such as the density dependence of nuclear symmetry energy [45]. It also affects various characteristics of neutron stars, including tidal deformation and the mass-radius correlation [46–48]. The high-momentum distribution of atoms in ultracold atomic gases, described through Tan's contact, is predominantly influenced by short-range pairs of distinct fermions, diminishing proportionally to k^{-4} [49–51]. Similarly, the NMD above the Fermi momentum is dominated by short-range correlated np pairs in the nucleus. By analyzing the experimental $(e, e'p)$ data and *ab initio* calculations of $n(k)$, an approximate $1/k^4$ behavior of $n(k)$ is observed in the region $0.325 < k < 0.625$ GeV/c [45]. Another investigation on the superscaling analysis for the inclusive cross sections finds that the high-momentum tail scales as $n(k) \sim 1/k^{8.5}$ [52].

It is shown in Fig. 5 that the new NMDs extracted from different inclusive cross sections present consistent results at high momenta. Consequently, the scaling behaviors of high-momentum tails are expected to be determined by fitting the new $n(k)$ results. The fitting outcomes are presented in Fig. 6. Like the results of Refs. [45,52], it is hypothesized that the NMD scales as $1/k^\alpha$ and high-momentum regions are divided into two parts, $0.25 < k < 0.6$ GeV/c and

$0.6 < k < 1.2$ GeV/c. Applying a fitting procedure to the $n(k)$ results within the region $0.25 < k < 0.6$ GeV/c leads to $1/k^5$ scaling. The orange band depicts the loci of the 95% confidence bound of the fitting. By fitting the $n(k)$ results at higher momentum regions above 0.6 GeV/c, the scaling behavior of $1/k^7$ provides the best coincidence. Due to slight deviations in the extracted $n(k)$ results at $0.6 < k < 1.2$ GeV/c, a relatively broad 95% confidence bound, the green band in the figure, is obtained in the fitting procedure.

To further signify the scaling behaviors of NMDs, we plot the scaled NMD in Fig. 7. The scaled NMD is defined as $k'^5 n(k')$ in Fig. 7(a) and $k'^7 n(k')$ in Fig. 7(b), where $k' = k/k_F$ with $k_F = 250$ MeV, the typical Fermi momentum for medium and heavy nuclei. It should be noted that the selection of k_F affects the normalization, but the extraction of scaling behaviors is not impacted. The region $1.0 < k' < 2.4$ in Fig. 7(a) corresponds to $0.25 < k < 0.6$ GeV/c for $k'^5 n(k')$ and the region $2.4 < k' < 4.8$ in Fig. 7(b) corresponds to $0.6 < k < 1.2$ GeV/c for $k'^7 n(k')$. Inspecting Fig. 7(a), a plateau $k'^5 n(k') = 0.700 \pm 0.019$ is observed for $1.0 < k' < 2.4$. Figure 7(b) also shows a plateau $k'^7 n(k') = 3.710 \pm 0.395$ for $2.4 < k' < 4.8$. The light red bands represent the 95% confidence bounds of the linear fitted curves. The existence of plateaus further verifies the piecewise scaling behaviors of NMDs. It is indicated in Ref. [4] that, in the region above k_F, the tensor force predominantly influences NMDs in the region $k < 0.6$ GeV/c, while the short-range repulsion dominates the higher-momentum region. We propose that varying dominance of short-range correlations in different k regions may underlie the piecewise scaling phenomena observed in NMDs. Although the correlated nucleons with high-k values account for a small fraction in nuclei, considering them in investigations on nuclear matters may yield different results.

IV. CONCLUSIONS

In summary, we utilize a modern numerical differentiation technique known as smoothing spline to extract NMDs of deuteron from the inclusive cross section data within the framework of y scaling. Traditionally, the NMDs extracted with the help of the finite difference approach may lead to negative values and suspect fluctuations at high momenta. It is shown that smoothing spline, which has a number of advantages over the traditional approach, gives NMDs more compatible with physical considerations. We extract new NMDs for the deuteron and study their scaling behaviors with respect to the nucleon momentum k. It is found that NMDs may follow piecewise scaling laws with $n(k) \sim 1/k^5$ for $0.25 < k < 0.6$ GeV/c and $n(k) \sim 1/k^7$ for $0.6 < k < 1.2$ GeV/c. These results may be also helpful for understanding the origin of the European Muon Collaboration effect [53,54], neutrinoless double-beta decay matrix elements [55], neutron stars [56], and relativistic heavy-ion collisions [57].

ACKNOWLEDGMENTS

This work is supported by the National Natural Science Foundation of China (Grants No. 12035011, No. 11975167, No. 11947211, No. 11905103, No. 11881240623, No. 11961141003, and No. 12375122), and by the National Key R&D Program of China (Contract No. 2023YFA1606503).

[1] R. B. Wiringa, R. Schiavilla, S. C. Pieper, and J. Carlson, Phys. Rev. C **89**, 024305 (2014).
[2] D. Lonardoni, S. Gandolfi, X. B. Wang, and J. Carlson, Phys. Rev. C **98**, 014322 (2018).
[3] L. E. Marcucci, F. Sammarruca, M. Viviani, and R. Machleidt, Phys. Rev. C **99**, 034003 (2019).
[4] M. Lyu, T. Myo, H. Toki, H. Horiuchi, C. Xu, and N. Wan, Phys. Lett. B **805**, 135421 (2020).
[5] X. Wang, Q. Niu, J. Zhang, M. Lyu, J. Liu, C. Xu, and Z. Ren, Sci. China Phys. Mech. Astron. **64**, 292011 (2021).
[6] J. Arrington *et al.*, Phys. Rev. Lett. **82**, 2056 (1999).
[7] O. Benhar, D. Day, and I. Sick, Rev. Mod. Phys. **80**, 189 (2008).
[8] N. Fomin *et al.*, Phys. Rev. Lett. **108**, 092502 (2012).
[9] M. Murphy *et al.* (The Jefferson Lab Hall A Collaboration), Phys. Rev. C **100**, 054606 (2019).
[10] D. Nguyen, Z. Ye, P. Aguilera *et al.*, Phys. Rev. C **102**, 064004 (2020).
[11] T. Liang, Z. Ren, D. Bai, and J. Liu, Phys. Rev. C **106**, 054324 (2022).
[12] G. B. West, Phys. Rep. **18**, 263 (1975).
[13] D. B. Day, J. S. McCarthy, T. W. Donnelly, and I. Sick, Annu. Rev. Nucl. Part. Sci. **40**, 357 (1990).
[14] K. S. Kim and L. E. Wright, Phys. Rev. C **76**, 044613 (2007).
[15] G. D. Megias, J. E. Amaro, M. B. Barbaro, J. A. Caballero, and T. W. Donnelly, Phys. Rev. D **94**, 013012 (2016).
[16] M. V. Ivanov, A. N. Antonov, and J. A. Caballero, Nucl. Phys. A **1003**, 122029 (2020).
[17] Q. Niu, J. Liu, Y. Guo, C. Xu, M. Lyu, and Z. Ren, Phys. Rev. C **105**, L051602 (2022).
[18] L. Wang, Q. Niu, J. Zhang, J. Liu, and Z. Ren, Sci. China Phys. Mech. Astron. **66**, 102011 (2023).
[19] C. Ciofi degli Atti, Phys. Rep. **590**, 1 (2015).
[20] C. Ciofi degli Atti, E. Pace, and G. Salmè, Phys. Rev. C **43**, 1155 (1991).
[21] Q. Meng, Z. Lu, and C. Xu, Phys. Rev. C **108**, 014001 (2023).
[22] M. Piarulli, S. Pastore, R. B. Wiringa, S. Brusilow, and R. Lim, Phys. Rev. C **107**, 014314 (2023).
[23] C. H. Reinsch, Numer. Math. **10**, 177 (1967).
[24] P. H. C. Eilers, Anal. Chem. **75**, 3631 (2003).
[25] K. Ahnert and M. Abel, Comput. Phys. Commun. **177**, 764 (2007).
[26] P. Barak, Anal. Chem. **67**, 2758 (1995).
[27] K. Gao and O. Sener, in *Proceedings of the 39th International Conference on Machine Learning*, 17–23 July 2022, edited by K. Chaudhuri *et al.* (PMLR, 2022), pp. 7077–7101.
[28] P. Craven and G. Wahba, Numer. Math. **31**, 377 (1978).
[29] J. J. Stickel, Comput. Chem. Eng. **34**, 467 (2010).
[30] M. D'Amico and G. Ferrigno, Med. Biol. Eng. Comput. **30**, 193 (1992).

[31] M. Kot, *Elements of Mathematical Ecology* (Cambridge University Press, Cambridge, 2001).
[32] F. Van Breugel, J. N. Kutz, and B. W. Brunton, IEEE Access **8**, 196865 (2020).
[33] T. De Forest, Jr., Nucl. Phys. A **392**, 232 (1983).
[34] J. Arrington, W. Melnitchouk, and J. A. Tjon, Phys. Rev. C **76**, 035205 (2007).
[35] J. J. Kelly, Phys. Rev. C **70**, 068202 (2004).
[36] C. C. degli Atti and G. B. West, Phys. Lett. B **458**, 447 (1999).
[37] J. A. Caballero, M. B. Barbaro, A. N. Antonov, M. V. Ivanov, and T. W. Donnelly, Phys. Rev. C **81**, 055502 (2010).
[38] J. Ryckebusch, W. Cosyn, S. Stevens, C. Casert, and J. Nys, Phys. Lett. B **792**, 21 (2019).
[39] G. Wahba, J. R. Stat. Soc. Ser. B **45**, 133 (1983).
[40] P. G. Reinhard, X. Roca-Maza, and W. Nazarewicz, Phys. Rev. Lett. **127**, 232501 (2021).
[41] M. B. Barbaro, J. A. Caballero, T. W. Donnelly, and C. Maieron, Phys. Rev. C **69**, 035502 (2004).
[42] M. C. Martínez, J. A. Caballero, T. W. Donnelly, and J. M. Udías, Phys. Rev. C **77**, 064604 (2008).
[43] G. D. Megias, T. W. Donnelly, O. Moreno, C. F. Williamson, J. A. Caballero, R. González-Jiménez, A. De Pace, M. B. Barbaro, W. M. Alberico, M. Nardi, and J. E. Amaro, Phys. Rev. D **91**, 073004 (2015).
[44] A. De Pace, M. Nardi, W. M. Alberico, T. W. Donnelly, and A. Molinari, Nucl. Phys. A **741**, 249 (2004).
[45] O. Hen, B.-A. Li, W.-J. Guo, L. B. Weinstein, and E. Piasetzky, Phys. Rev. C **91**, 025803 (2015).
[46] H. Lu, Z. Ren, and D. Bai, Nucl. Phys. A **1011**, 122200 (2021).
[47] B. Hong, Z. Ren, C. Wu, and X. Mu, Class. Quantum Grav. **40**, 125007 (2023).
[48] X. Shang, P. Wang, W. Zuo, and J. Dong, Phys. Lett. B **811**, 135963 (2020).
[49] S. Tan, Ann. Phys. (NY) **323**, 2952 (2008).
[50] S. Tan, Ann. Phys. (NY) **323**, 2971 (2008).
[51] S. Tan, Ann. Phys. (NY) **323**, 2987 (2008).
[52] A. N. Antonov, M. V. Ivanov, M. K. Gaidarov, and E. Moya de Guerra, Phys. Rev. C **75**, 034319 (2007).
[53] O. Hen, E. Piasetzky, and L. B. Weinstein, Phys. Rev. C **85**, 047301 (2012).
[54] H. Dai, R. Wang, Y. Huang, and X. Chen, Phys. Lett. B **769**, 446 (2017).
[55] M. Kortelainen, O. Civitarese, J. Suhonen, and J. Toivanen, Phys. Lett. B **647**, 128 (2007).
[56] L. A. Souza, M. Dutra, C. H. Lenzi, and O. Lourenço, Phys. Rev. C **101**, 065202 (2020).
[57] W.-M. Guo, B.-A. Li, and G.-C. Yong, Phys. Rev. C **104**, 034603 (2021).